Field-induced columnar transition of biocompatible magnetic colloids: An aging study by magnetotransmissivity

M. T. A. Eloi,[1] J. L. Santos, Jr.,[2] P. C. Morais,[1] and A. F. Bakuzis[2,*]
[1]*Instituto de Física, Núcleo de Física Aplicada, Universidade de Brasília, Brasília, DF 70910-900, Brazil*
[2]*Instituto de Física, Universidade Federal de Goiás, Goiânia, GO 74001-970, Brazil*
(Received 29 July 2009; revised manuscript received 5 January 2010; published 24 August 2010)

The field dependence of the optical transmission of tartrate-coated and polyaspartate-coated magnetite-based aqueous colloids was studied. The colloidal stock samples were diluted to prepare a series of samples containing different particle volume fractions ranging from 0.17% up to 1.52% and measured at distinct times after preparation (1, 30, 120, 240, and 1460 days). We show that the magneto-transmissivity behavior is mainly described by the rotation of linear chains, at the low-field range, whereas the analysis of the data provided the measurement of the average chain length. Results also reveal that the optical transmissivity has a minimum at a particular critical field, whose origin is related to the onset of columns of chains built from isolated particle chains, i.e., due to a columnar phase transition. We found the critical field reducing as the particle volume fraction increases and as the sample's aging time increases. To investigate the origin of this phenomenon we used phase condensation models and Mie's theory applied to a chain of spheres and to an infinite cylinder. Possible implications for magnetophotonic colloidal-based devices and biomedical applications were discussed.

DOI: 10.1103/PhysRevE.82.021407 PACS number(s): 83.80.Hj, 75.50.Mm, 42.25.Bs, 78.20.Ls

I. INTRODUCTION

Magnetic colloids (also termed magnetic fluids or ferrofluids), consisting of nanosized magnetic particles stably dispersed in a polar or nonpolar liquid carrier, provide the material platform for a broad range of applications, ranging from magneto-optical devices up to cancer diagnosis and treatment [1–8]. Magneto-optical devices include optical switches, isolators, fiber sensors, and modulators [3–6]. In fact, several studies, as for instance light scattering in magnetic colloids (MCs), date from more than 10 years ago [9–11]. Nowadays, there is a great deal of interest in using such material system for building magnetophotonic devices since photonic properties, such as backward and forward scattering, might be magnetically controlled [12–19]. Interesting results have been recently reported by Mehta *et al.* [13] regarding the zero forward scattering in magnetorheological fluids and by Philip *et al.* [15] and Cintra *et al.* [19] on field-induced extinction of light in magnetic fluids (MFs). Indeed, Laskar *et al.* [16] suggested the onset of Mie's resonances to explain the appearance of a minimum in the field dependence of the light transmissivity in MCs. Understanding the origin of such phenomena might lead to new opportunities for magnetophotonic applications.

On the other hand, investigation of magneto-optical properties of MCs is extremely interesting from the fundamental point of view, as for instance in the investigation of phase transition phenomena, which are related to the onset of bulk droplike and/or columnar structures [20–41]. In fact, it is well known that when MCs are subjected for instance to magnetic fields, reducing temperature or increasing ionic strength, the fluid can undergo a phase transition [20–24], which has been theoretically treated as a "gas-liquid" transition by several authors [27–33]. Basically, what is obtained from the models employed is the occurrence of a critical parameter value (field, ionic strength, particle volume fraction, temperature) above (or below), which phase separation takes place. However, depending on the theoretical approach used, as for example the use of the lattice gas model or a Carnahan-Starling model [27,33] while describing the fluid entropy, the critical concentration above which the phenomenon occurs can be quite different. Also, the investigated MCs may present nanoparticles which are polydisperse in size. As a consequence, in some cases, a better representation of the experiments can only be achieved assuming that polydisperse systems can be represented, essentially, as a bidisperse system, containing a large fraction of small particles mixed with a small fraction of large particles [42]. The presence of large particles within MCs plays a key role on the phase condensation phenomena. Finally, it is interesting to notice that the models used to describe the "gas-liquid" transition usually predict that the presence of linear chains within the MC system prevents the occurrence of the phase transition [35]. Further, since MC can change into solidlike state under magnetic field, biocompatible samples could be used to block the blood flow to a localized tumor, starving the cancer cells of their blood supply, causing their death. Such idea has been suggested before by Liu *et al.* using magnetorheological fluids, which unfortunately have larger particle sizes [43–45]. Therefore, the comprehension of the phase transition process should be also very useful in the biomedical field.

Indeed, small aggregates, usually linear chains, are known to spontaneously form within MCs. Probably, the first discussion about small agglomerates in MCs was related to studies investigating the origin of magnetic birefringence [46]. More recently, however, there are several theoretical and experimental works confirming the existence of agglomerates and evaluating the effect of linear chains and/or other

*Corresponding author; bakuzis@if.ufg.br

structures on the rheological, magnetic, magneto-optical, among others properties [2,35–39,47–62]. As for instance, 2D cryogenic transmission electron microscopy study performed on MFs have evidenced the appearance of a columnar phase transition, which includes a "solidlike phase" in the sense that several chains of nanoparticles bind together to form thick cylinderlike objects [20,37,38]. While trying to answer the question of how the presence of these structures, field-induced or pre-existing agglomerates, changes the properties of MCs, in particular the phase condensation process, we found the understanding of this subject still at its infancy. In fact, differently from the classical condensation phase transition [35], only recently Iskakova *et al.* [36] had theoretically concluded that the appearance of linear chains within MCs can precede the particle bulk condensation. The theoretical conclusion agrees not only with the experiments of Goldberg *et al.* [20] and Klokkenburg *et al.* [37,38], performed on two-dimensional (2D) MF films, but also with a MF resonance study reported by Skeff Neto *et al.* [63].

Since it is well known that magneto-optical effects are extremely sensitive to pre-existing and/or field-induced particle chain [2,46,57,64–66] one easily get into the conclusion that magneto-optical effects might be useful to study several phenomena in MCs, as for instance phase transitions. In this study we used a magneto-transmissivity technique to investigate the aging of biocompatible MCs, which have important biomedical applications in regard to the diagnosis and treatment of diseases [1,67,68]. The experimental setup, although simple, has been seldom used in the investigation of MCs [15,16,19,26,65]. The data provided by the measurements together with our theoretical analysis allowed us to study field-induced extinction of light in MCs [15,19] while connecting the phenomenon to a field-induced three-dimensional columnar transition [10,37,69–71]. Further, previous studies have suggested that the occurrence of a minimum on the field dependence of the magneto-transmissivity is correlated with Mie's resonances due to field induced particle chain formation [15,16]. In addition, it was argued that the mechanism behind the Mie's resonances was due to ferromagnetic scatterers. The idea of ferromagnetic scatterers [12] is very interesting indeed and certainly important at specific wavelengths. However, at optical wavelengths, the magnetic permeability contribution to the extinction cross section is negligible. Therefore, in order to improve our understanding of the phenomenon and check whether noninteracting nanoparticle chains could be responsible or not for the existence of the minimum in the optical transmissivity, we applied the Mie's theory [72–74] to a chain of spheres. As far as we know, this is the first time that such procedure appears in the literature. In our approach, ferromagnetic scatterers do not give any contribution.

Since the presence of structures, such as aggregates and cylinderlike objects, can shift the Mie resonance position, the comprehension of the phenomenon might be useful for several nanophotonic-based systems, where self-organization plays an important role. In fact the kind of investigation that will be reported here could be useful for other nanoparticle-based colloids, such as: (i) metal nanoparticles (usually gold and silver), which has potential biomedical application through the phenomenon of plasmonic hyperthermia [75,76], as well as technological ones, since it might be possible to use them as optical metamaterials [77,78]; (ii) or core-shell nanoparticles, which consist of a magnetic core and a metallic shell nanoparticle [79–81]. Although in our present work, we had not analyzed metallic or core-shell nanoparticle colloids, it is noticeable that self-organizated structures, such as chains and cylinderlike objects, can have important impact on biomedical—through a shift in the plasmonic resonance position—and magnetophotonic applications.

In this study, we will show that the phenomenon of the extinction of light in MCs is related to the rotation of pre-existing and/or field-induced agglomerates. However, the existence of a minimum in the magneto-transmissivity data is actually related to the columnar phase transition. Such conclusion has important implications for the biomedical field. As for instance, an important situation where this phenomenon should be considered is in the biomedical application associated to the use of magnetizable stents, which consists of metal structures used to treat coronary artery disease [82,83]. The idea is that magnetizable stents could work as platforms to target magnetic drug delivery nanocarriers. One important thing that should be controlled at this application is the formation of self-organized structures, chains and specially columnar structures, since those structures could promote arterial and capillary embolization. Those situations are not desirable in target drug delivery systems. On the other hand, there could be situations where magnetic stents together with magnetic nanocarriers might be used to block the blood flow to a localized tumor as discussed before [43–45].

Our study has investigated two types of surface coating layers for spherical nanosized magnetite particles; tartrate and polyaspartate molecular species, the latter one being a polymer. In addition, we followed the magneto-optical properties of the MCs as a function of time. Other aging studies involving MCs, although quite rare, can be found in the literature [84–86], but usually the period of investigation is not as long as the period spent in the present study (240 days). Such kind of investigation is very important while using MCs for any technological, biomedical, or other kinds of application.

This paper is organized in the following way. First, we discuss the synthesis of the MC samples, the nanoparticle characterization, and the optical experimental setup (Sec. II). In Sec. III, we introduce the magneto-transmissivity model. Section IV is devoted to the presentation of the experimental data, revealing that the extinction of light in MCs is related to the rotation of pre-existing and/or field-induced agglomerates. The chain size of the self-organized structures was modeled using theoretical approaches from the literature and we found them to be time dependent. The critical fields were analyzed within the framework of two existing models. The first model has been used on traditional phase condensation studies (Ivanov bidisperse model) [42] whereas the second one has been applied in the description of "solidlike" transitions [71]. Besides these approaches we also included a cross section theoretical analysis using the Mie's theory [72,73]. The Mie's theory approach allowed us to conclude that the minimum observed in the magneto-transmissivity data can actually be attributed to the columnar phase transition. Finally, Sec. V presents our conclusions.

II. SAMPLE PREPARATION AND EXPERIMENTAL SETUP

A. Sample preparation

Tartrate-coated magnetite-based magnetic fluid—referred as TMF sample in the text—was produced as described in the literature [87,88]. Nanosized magnetite was coprecipitated from a mixture of Fe^{+2} and Fe^{+3} using ammonia solution. The dispersion was stirred at 75 °C for 30 min in order to achieve the magnetite crystal formation. Then, the particles were magnetically separated and washed with distilled water up to 8 times to remove ammonia excess. Hydrochloric acid was added to the dispersion in order to reduce the pH down to 2, thus forming a stable magnetite hydrosol. In the sequence, tartaric acid sodium salt water solution was added to the magnetite hydrosol with constant stirring. For the complexation of magnetite cores with tartrate groups, the dispersion was heated for 30 min at 50 °C. At the end of this process a pH2 unstable dispersion was obtained. To remove tartrate excess from the reaction medium the particles were magnetically separated and washed with distilled water. In addition, the as-produced sample was maintained under sonication for a very short time (5 min). Slight sonication was employed in order to avoid complete disruption of small agglomerates within the sample, since our interest was the investigation of agglomerates through aging and the sonication procedure might interfere with aging effects. For neutralization and colloidal stabilization of the suspension, the pH value was gradually increased up to 7.5 by adding potassium hydroxide water solution. Finally, the dispersion was filtered through glass fibers twice, obtaining a stable MF sample (TMF) dispersed at pH7 and physiological condition (0.9% NaCl). A similar procedure was applied to obtain the polyaspartate-coated magnetite-based magnetic fluid sample (PMF sample), as described in the literature [88].

B. Nanoparticle characterization

The particle size polydispersity profile of the TMF sample (see Fig. 1) was obtained from transmission electron microscopy (TEM) micrographs using the Jeol JEM-3010 ARP microscope, operating at 300 kV (resolution 1.7 Å), from which were found the modal magnetic core diameter (D_M=7.17 nm) and the size dispersity (σ=0.24), assuming the lognormal distribution function $P(D)=\exp^{-\sigma^2/2}/(\sqrt{2\pi}D_M\sigma)\exp[-\ln^2(D/D_M)/(2\sigma^2)]$. The particle volume fraction (ϕ) associated to the TMF sample was calculated using $\phi=n(\pi/6)\int D^3P(D)dD$, where n is the number of particles per unit volume, obtained from atomic absorption analysis, and $P(D)$ the particle diameter distribution. The insets of Fig. 1 show a high-resolution TEM picture (left panel) and the powder x-ray diffraction (XRD) (right panel) of the nanosized magnetite recorded with the Shimadzu XRD 6000 spectrometer using the Cu-Kα radiation. The particle volume fraction of the TMF stock sample, taking into account only the magnetic core, was found to be 1.9%. The TMF stock sample was diluted using physiological solution in order to produce samples with different particle volume fractions (0.17%, 0.35%, 0.70%, and 1.38%) for investigation 1, 30, 120, and 240 days after preparation.

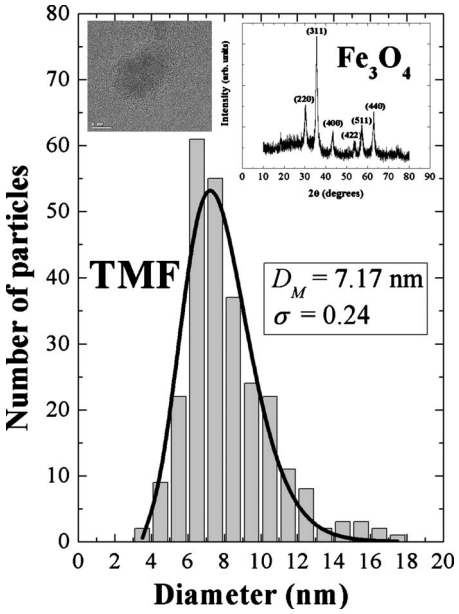

FIG. 1. Diameter distribution of the magnetic particles of TMF samples obtained from transmission electronic microscopy. The left panel shows a picture of a typical high-resolution TEM picture. At the right panel, the x-ray diffraction of nanoparticles indicates the spinel structure of magnetite.

In order to compare the influence of the surfactant layer in the experiment we also analyzed data obtained from the polyaspartate-coated magnetite-based magnetic fluid sample (PMF), whose characterization was already reported in Ref. [19]. The PMF stock sample (3.04% coated-particle volume fraction), containing particles with modal magnetic core diameter of 8.42 nm and size dispersity of 0.31 (lognormal distribution function), was diluted in order to produce a series of samples with different volume fractions (0.38%, 0.61%, 1.03%, and 1.52%) for investigation 240 days after preparation.

C. Optical experimental setup

The field dependence of the optical transmission of the MC samples presenting different particle volume fractions and aging times was investigated using the experimental setup shown schematically in Fig. 2. The sets of diluted TMF samples were evaluated 1, 30, 120, and 240 days after preparation. For comparison, the PMF samples were also evaluated 240 days after preparation. Room-temperature magneto-transmissivity data were obtained using the traditional lock-in detection technique. The experimental setup (see Fig. 2) consists of a 10 mW chopped laser beam (λ=632 nm) crossing perpendicularly the sample cell before illumination of the photo detector. The flat quartz sample cell has an internal sample thickness (l) of 1 mm. Both polarizer and analyzer are attached to a goniometer device that allows full angular rotation. The sample cell is mounted in the gap of an electromagnet so that the laser beam and the external magnetic field are mutually perpendicular. The axes of the polar-

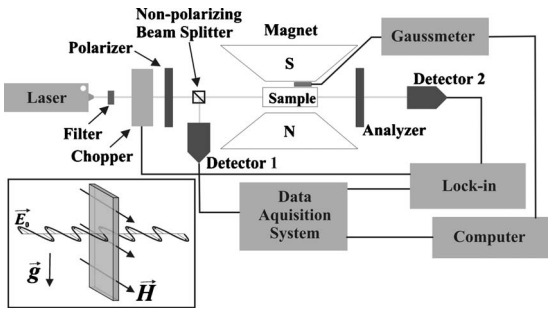

FIG. 2. Experimental setup for magneto-transmissivity measurements. The inset shows a 3D representation of the sample holder, polarization of electric field of incident light ($\vec{E}_0$), applied magnetic field ($\vec{H}$), and gravity ($\vec{g}$).

izer and analyzer are set both parallel to the magnetic field direction. Then, an absorption filter is positioned before the polarizer with the purpose of avoiding thermodiffusion effects. A non-polarizing beam splitter, placed after the polarizer, directs a reference beam to another detector, rectifying occasional laser oscillations. In our experimental configuration gravity is parallel to one of the major lengths of the sample cell (see inset of Fig. 2), whereas it points along the sample thickness in most reported studies [14,16,71]. Such experimental configuration is interesting since columnar structures can be easily observed [19].

III. THEORETICAL MODEL

Considering a flat colloid-based film of thickness l the outgoing light intensity (I) of a perpendicularly incident light beam of intensity I_0 is given by $I=I_0\exp(-nC_{ext}l)$, where $n=\phi/v$, v is the particle volume and C_{ext} is the extinction cross section, the sum of absorption (C_{abs}) and scattering (C_{sca}) ones. Within the first-order approximation of Mie's theory for spherical particles with sizes smaller than the light wavelength (λ), cross sections depend on particle electric polarizability (α) according to $C_{abs}=k\,\mathrm{Im}\{\alpha\}$ and $C_{sca}=k^4|\alpha|^2/(6\pi)$, where $k=2\pi/\lambda$ and Im{} denotes imaginary part of the argument [73]. According to the Clausius-Mossotti's equation, the electric polarizability of a sphere (α_s) and its electric polarizability per unit volume (χ_s) are given by $\alpha_s=\chi_s v=3v(\varepsilon_1-\varepsilon_m)/(\varepsilon_1+2\varepsilon_m)$, where ε_1 and ε_m are the electric permittivity of the suspended particle and the carrier liquid, respectively. Taking into account the surfactant layer electric permittivity (ε_2) and the thickness of the surface coating (δ) the electric polarizability of the surface-coated sphere (α_{cs}) becomes [73]:

$$\alpha_{cs}=\chi_{cs}v=3v\frac{(\varepsilon_2-\varepsilon_m)(\varepsilon_1+2\varepsilon_2)+f(\varepsilon_1-\varepsilon_2)(2\varepsilon_2+\varepsilon_m)}{(\varepsilon_2+2\varepsilon_m)(\varepsilon_1+2\varepsilon_2)+f(\varepsilon_1-\varepsilon_2)(2\varepsilon_2-2\varepsilon_m)}, \tag{1}$$

where $f=(1+2\delta/D)^{-3}$ is the ratio between the particle core volume and the whole sphere, as long as v in the above equation states for the volume of the surface-coated sphere. For $\lambda=632$ nm, the magnetite electric permittivity is $\varepsilon_1=5.2+3.0i$ [89] whereas the water electric permittivity is $\varepsilon_m=1.78$ [73]. ε_2 for tartrate and polyaspartate layers are 2.25 and 2.76, respectively [90]. For a magnetite sphere with a diameter of 7.2 nm suspended in water, scattering cross section is more than three orders of magnitude smaller than absorption one, permitting us to replace C_{ext} by C_{abs}.

Within a carrier liquid stably-suspended magnetic nanoparticles tend to form dimers, trimers, or even longer chains [52–56,91–93]. Thus, in the present study, the electric polarizability of an aggregate of nanosized particles was modeled as a linear chain of spheres. According to the oscillating dipole model [92], the electric polarizability per unit volume of a chain of Q spherical particles, referred to a coordinate system where the z' axis connects the center of the particles, is given by the following diagonal tensor:

$$\overleftrightarrow{\chi}'_Q=\begin{pmatrix}\chi_Q^{xx} & 0 & 0\\ 0 & \chi_Q^{yy} & 0\\ 0 & 0 & \chi_Q^{zz}\end{pmatrix},$$

with

$$\chi_Q^{xx}=\chi_Q^{yy}=Q^{-1}\sum_{j=1}^{Q}\chi_{cs}/(1+\kappa_j\chi_{cs})$$

and

$$\chi_Q^{zz}=Q^{-1}\sum_{j=1}^{Q}\chi_{cs}/(1-2\kappa_j\chi_{cs}), \tag{2}$$

where $\kappa_j=(1/24)(1+s/D)^{-3}\Sigma_{i\neq j}^{Q}|i-j|^{-3}$, s is the surface-to-surface separation between neighboring particles, and D is the nanoparticle diameter.

The electric polarizability per unit volume of a chain of Q spherical particles in the laboratory coordinate system ($\overleftrightarrow{\chi}_Q$) can be obtained by a second rank tensor transformation $\overleftrightarrow{\chi}_Q(\theta,\varphi)=R(\theta,\varphi)\overleftrightarrow{\chi}'_Q R^{-1}(\theta,\varphi)$, where R is the rotation matrix described in terms of the spherical angles θ and φ. Under the action of an external magnetic field $\vec{H}$ the magnetic, the dipole moments of magnetic nanosized particles tend to align parallel to the applied field. Assuming that the orientation of the particles follows a Boltzmann distribution and $\vec{H}$ lays along the x axis, the Boltzmann factor is $\exp(-\mu_0 QmH\sin\theta\cos\varphi/k_BT)$, where μ_0, m, k_B and T are the vacuum magnetic permeability, the magnetic dipole of an isolated nanoparticle, the Boltzmann constant and the absolute temperature, respectively. The magnetic dipole moment of a spherical nanoparticle is $m=(\pi/6)D^3M_s$, where M_s is the nanoparticle saturation magnetization. In the laboratory coordinate system each type of aggregate is described by the following average electric polarizability per unit volume:

$$\langle\overleftrightarrow{\chi}_Q\rangle=\frac{\int\int\overleftrightarrow{\chi}_Q\exp(\mu_0 QmH\sin\theta\cos\varphi/k_BT)d(\cos\theta)d\varphi}{\int\int\exp(\mu_0 QmH\sin\theta\cos\varphi/k_BT)d(\cos\theta)d\varphi}. \tag{3}$$

In order to solve the integrals in $d\varphi$ we shall take a cyclic permute of xyz into zxy. After integration over all orienta-

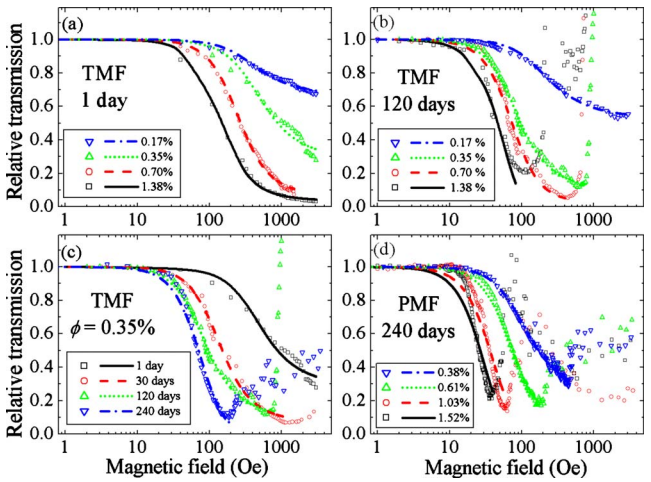

FIG. 3. (Color online) Symbols show normalized parallel transmissivity $t_{\parallel}$ as function of magnetic field for: (a) One-day-old TMF samples, (b) 120-day-old TMF samples, (c) TMF samples possessing ϕ=0.35% at different aging times, and (d) 240-day-old PMF samples, obtained from Ref. [19]. In the four panels, lines state the best fitting obtained from the model [see Eq. (5)] up to critical field.

tions and considering an x-polarized incident light only the xx component would remain and the average electric polarizability per unit volume of all particles in the laboratory coordinate system is found to be:

$$\langle \overleftrightarrow{\chi_Q} \rangle = \langle \chi_Q \rangle = \frac{\chi_Q^{zz} + 2\chi_Q^{xx}}{3} + \frac{2}{3}(\chi_Q^{zz} - \chi_Q^{xx}) L_2(\xi_Q), \qquad (4)$$

where $L_2(\xi_Q)=1-3\mathrm{L}(\xi_Q)/\xi_Q$ is the second-order Langevin function, with $L(\xi_Q)=1/\tanh(\xi_Q)-1/\xi_Q$ and the argument $\xi_Q=Q\mu_0 mH/(k_B T)$.

Moreover, considering the presence of chainlike structures of different sizes (Q) within the magnetic colloid sample and defining ϕ_Q as the volume fraction of the linear chain of Q surface-coated particles, the particle volume fraction is $\phi=\Sigma\phi_Q$. Thus, the parallel optical transmission $t_{\parallel}=I/I_0$ for a x-polarized light is given by:

$$\ln(t_{\parallel}) = -\frac{2\pi l}{\lambda} \sum_Q \phi_Q \, \mathrm{Im}\{\langle \chi_Q \rangle\}. \qquad (5)$$

Since $\mathrm{Im}\{\chi_Q^{zz}\} > \mathrm{Im}\{\chi_Q^{xx}\}$ for $Q>2$, as the applied field increases $t_{\parallel}$ is expected to decrease following a second-order Langevin function.

IV. RESULTS AND DISCUSSION

Symbols in all panels of Fig. 3 represent the magnetic field dependence of the normalized parallel transmission ($t_{\parallel}$). Normalization of $t_{\parallel}$ was performed with respect to the transmission value at zero applied field. Figure 3(a) shows the relative transmission (normalized parallel transmission) of the one-day-old TMF samples, revealing that transmissivity decreases systematically as the applied magnetic field increases. In addition, Fig. 3(a) shows that the higher the particle volume fraction (ϕ) the more pronounced the transmissivity decrease is. As shown in Fig. 3(b), the 120-day-old TMF samples reveal a similar behavior, except for the onset of a critical field (H_c), in which the relative transmission shows a minimum, also observed in the 30 and 240-day-old TMF samples (data not shown). Furthermore, note from Fig. 3(b) that the critical field value shifts downwards as the particle volume fraction increases. Figure 3(c) shows the relative transmission of the ϕ TMF sample at increasing aging times, revealing that older samples present an earlier decrease in relative transmission whereas shifting the critical field toward lower field values. These findings suggest that C_{ext} is strongly dependent upon the aging time while raises the question of which mechanisms should be responsible for the onset and shift of the critical field. For comparison, Fig. 3(d) shows the relative transmission of the 240-day-old PMF samples, already published in Ref. [19], but not analyzed within the approach presented here. Similarly, data on Fig. 3(d) also show a decrease in relative transmission down to a minimum at different critical field values which scales with the sample particle volume fraction. Indeed, samples TMF and PMF present the same relative transmission behavior as far as the aging time and particle volume fraction are concerned.

In order to explain the experimental data, we first focused on the relative transmission behavior at fields lower than H_c (see Fig. 3). The origin of the critical field is discussed later on in the text. Solid lines in Figs. 3(a)–3(d) are the best fit of the data using Eq. (5). In our analysis the surface-to-surface distance (s) was set to zero, since it is reasonable to argue that neighboring particles in a chain are touching one another. From a simple geometrical method, based on molecular orbitals, we estimated the thickness of the tartrate layer on the particle's surface around 0.55 nm. Likewise, the polyaspartate layer on the particle's surface was estimated around 3.0 nm in thickness. As the extinction process depends on the particle volume fraction, we used for samples TMF the average particle diameter of $\bar{D}=\sqrt[3]{\int D^3 P(D) dD}=8.28$ nm. For PMF samples, however, we found $\bar{D}=10.7$ nm instead. In order to minimize the number of fitting parameters we considered the presence of monodisperse particles, spherically shaped (not able to contribute to the magneto-optical effect), plus linear chains of average size Q_a. Basically, the model has to deal with just 2 parameters, Q_a and P_1, the latter representing the relative population of isolated particles ($P_1=\phi_1/\phi$). Note that the particle volume fraction of surface-coated particles is bigger than the particle volume fraction of surface-uncoated ones by a factor of $f^{-1}=(1+2\delta/\bar{D})^3$.

From the fitting procedure (see solid lines) shown in Figs. 3(a)–3(d), we concluded that the employed theoretical model was able to explain the decrease of the relative transmission as a function of the applied magnetic field for fields lower than H_c, indicating that field-induced alignment of preexisting linear chains can cause the observed extinction of light intensity. The proposed approach showed better fitting results for samples presenting lower particle volume fractions whereas slight deviations between the data and the fittings was observed for the more concentrated samples. This finding could be an indication of field-induced chain forma-

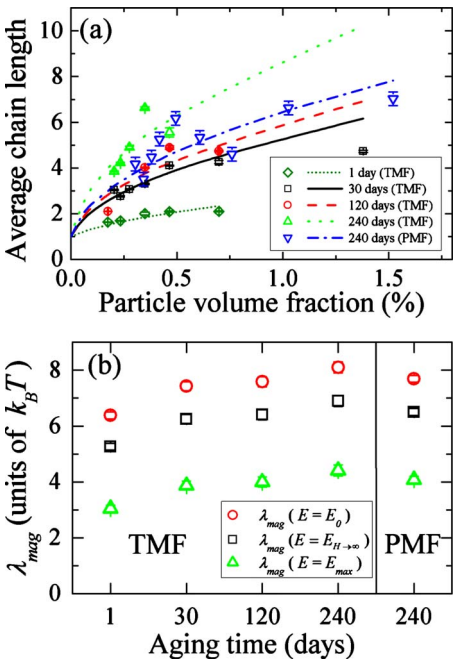

FIG. 4. (Color online) (a) Symbols denote average chain size $\langle Q\rangle$ acquired from fitting parameters as function of particle volume fraction. Lines state best adjustment of average chain length according to theoretical calculation [see Eq. (6)] for different days. (b) Symbols show dipolar magnetic coupling constant λ_{mag} obtained from fitting parameter E for no-applied field ($E=E_{H=0}$), infinity magnetic field ($E=E_{H\to\infty}$), and head-to-tail configuration ($E=E_{\max}$).

tion for samples presenting higher ϕ values. Therefore, we also modeled the experimental data considering the increase of the average chain length as a function of the applied field using the theoretical models described in Refs. [47,49]. However, in the range of particle volume fractions investigated we found a very tiny difference between the calculated chain size with and without applied field. Furthermore, while analyzing the fittings achieved with the TMF (nonpolymer coated) samples we found that the fittings obtained with the PMF (polymer coated) samples were poorer. This might be related to the presence of complex structures (rings or branched clusters) not considered in the present approach, appearing on MCs based on polymer coated nanosized particles in which the interaction between the surface coating species in neighboring particles can be more complicated.

Moreover, the approach used to fit the relative transmission data was able to provide information regarding the average chain length within the MC samples investigated. The particle volume fraction dependence of the average chain length, the latter defined as $\langle Q\rangle = P_1 + (1-P_1)Q_a$ and obtained from the fitting procedure, is represented by symbols in Fig. 4(a). Our findings regarding the TMF sample show that the average chain length has a tendency to increase with the increasing of both aging time and particle volume fraction. It is quite obvious the increasing of $\langle Q\rangle$ as the ϕ value increases, as already reported in the literature through experiments and calculations [47,49,52–56,92,93]. However, the finding that older samples present longer chains reveals that MC samples do not possess a static equilibrium as far as the chain length is concerned. The particle volume fraction dependence of the average chain length obtained for the 240-day-old PMF sample (see symbols) is also presented in Fig. 4(a). Lines (dotted, dashed, dot-dashed, solid) in Fig. 4(a) represent the fittings of the experimental data (symbols) according to the model described in the next paragraph.

The dependence of the average chain length on the volume fraction is described by [35,36,54]:

$$\langle Q\rangle = \frac{2\phi e^E}{\sqrt{1+4\phi e^E}-1}. \tag{6}$$

Equation (6) was first derived by Cebers, using the method of chemical equilibrium for the different types of aggregates [54]. By considering the MC as an ideal gas mixture of chains and minimizing its free energy, Zubarev and Iskakova obtained the same expression, where E is a dimensionless energy parameter of neighboring particles in a chain, normalized with respect to the thermal energy (k_BT) [35,36]. Lines in Fig. 4(a) represent the best fit of $\langle Q\rangle$ using Eq. (6). For zero applied field, one has $E_{H=0}=2\lambda_{mag}-\ln(3\lambda_{mag}^3)$, whereas $E_{H\to\infty}=2\lambda_{mag}-\ln(3\lambda_{mag}^2)$ represents the energy parameter at very strong fields [52,53]. Note that the interaction parameter $\lambda_{mag}=m^2/(D^3k_BT)$ represents the magnetic dipole-dipole coupling constant. Neglecting the chain entropy, we can also model E as the maximum dipolar attraction among two touching particles within the head-to-tail configuration as $E_{\max}=2\lambda_{mag}$ [47]. Figure 4(b) shows the λ_{mag} parameter (in units of k_BT) as a function of the samples' aging time obtained within the three particular cases discussed above, i.e., $E=E_{H=0}$, $E=E_{H\to\infty}$, and $E=E_{\max}$. Despite the excellent qualitative agreement, the values we found for the coupling constant (λ_{mag}) correspond to particle diameters ranging from 12.8 to 17.7 nm. It is possible that the λ_{mag} values we found are overestimated because other interaction terms were not included in the calculation of the chain length, which are extremely important at this particle size range, as for instance the van der Waals and the steric interactions [56]. Another possible reason, however, could be related to the particle size growth during the experimental running time. Nevertheless, we should stress that during the time window of our experiments (up to 240 days) we found no evidences of particle size growth in the MC samples investigated.

Due to the presence of surfactant molecules, the steric interaction among two neighboring surface-coated spheres is described by [94]:

$$\frac{E_S}{k_BT} = \begin{cases} 2\pi D^2\zeta\left[2-\dfrac{y+D}{\delta}\ln\left(\dfrac{2\delta+D}{y+D}\right)-\dfrac{y}{\delta}\right], & y\le 2\delta, \\ 0, & y>2\delta, \end{cases} \tag{7}$$

where ζ is the grafting coefficient, representing the surface density of molecular species, and y is the surface-to-surface separation distance between magnetic cores. Analysis of Eq. (7) shows that the smaller the distance y the stronger the steric repulsion (E_S). Note that in the head-to-tail configuration the dipole-dipole magnetic interaction is proportional to $(1+y/D)^{-3}$. Considering the magnetic dipole coupling con-

TABLE I. Dipole coupling constant (λ_{mag}), obtained from $E=E_{H\to\infty}$ case, and the estimated surface-to-surface distance between magnetic core of neighboring particles (y), considering that $y=2\delta$ for 1-day-old TMF samples.

Surfactant species	Aging time (days)	λ_{mag}	y (nm)
Tartrate	1	5.3	1.1
	30	6.3	0.57
	120	6.4	0.50
	240	6.9	0.29
Polyaspartate	240	6.5	6.0

stant obtained from $E_{H\to\infty}$ [see Fig. 4(b)] as an effective dipolar magnetic energy it is possible to estimate the time evolution of the surface-to-surface distance between spherical cores. The fitting parameter for infinite applied field was chosen because it is compatible with the head-to-tail alignment and provides values of λ_{mag} between the two limiting cases ($E_{\max}$ and $E_{H=0}$). Table I presents the estimated values of the surface-to-surface separation between neighboring particles, considering $y=2\delta$ for one-day-old samples. Data presented in Table I suggest that particles in a chain get closer together as the MC samples age, a clear indication that desorption of surfactant layers takes place upon samples' aging. Though the polyaspartate species are longer than the tartrate ones we found similar interaction energy for the two 240-day-old MC samples. This finding strongly indicates the contribution of additional particle-particle interaction terms not included in our approach, since bigger particles increase magnetic dipolar interaction whereas longer surfactant molecules assure stability with smaller aggregates.

We are now in position to investigate the origin of the critical field and its connection with particle chains. Symbols in Fig. 5(a) represent the critical field versus the particle volume fraction of TMF samples, at different aging times. Symbols in Fig. 5(b) compare the $H_c\times\phi$ data of TMF and PMF 240-day-old samples. Similar behavior can be found in the literature [15,19]. From our data two tendencies are observed: the older and the more concentrated the MC samples are the lower the critical fields observed. Philip *et al.* [15] have suggested that the critical field should follow a power law decay with respect to the particle volume fraction ($H_c\propto\phi^{-\beta}$), indicating that the observed structural phase transition is triggered by chain formation [15,16,71]. Further, the authors suggested that magnetic scatterers [12] are responsible for Mie's resonance, the reason for the minimum in transmissivity. According to scaling analysis the power law exponent (β) is expected to lie in between 0.25 and 0.75 [71]. Although our results can be fitted with a power law, the fittings provided critical exponents varying from 2.6 to 4.1 for the TMF samples and 2.1 for the PMF samples. Nevertheless, the values we found for β are much larger than the expected theoretical value for chain formation.

In order to investigate the role of isolated nanoparticle chains on the minimum of the transmissivity, we calculated the extinction efficiency, defined as the ratio between C_{ext} and orthogonal projected area of the sphere. Mie's extinction

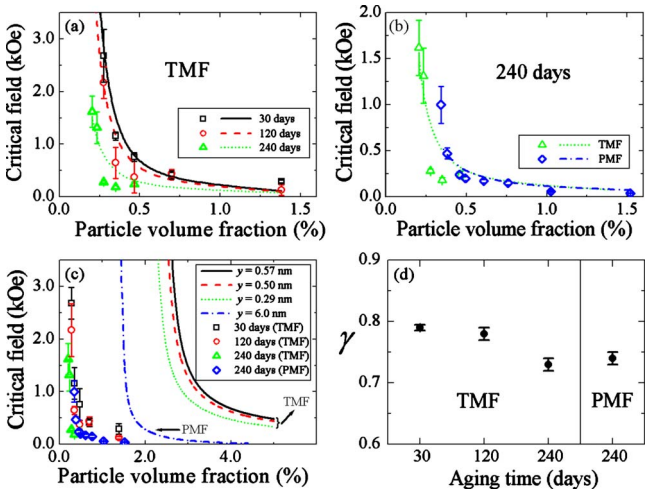

FIG. 5. (Color online) (a) Symbols show H_c as function of particle volume fraction for TMF samples at different aging times, and (b) for 240-day-old TMF and PMF samples. Lines are the fitting of experimental data according to the structural transition model [see Eq. (11)]. (c) Symbols reveal critical field as function of particle volume fraction for all samples. Phase diagrams (lines) estimate critical field as function of volume fraction according to Ivanov's model [42] for bidisperse magnetic fluids that simulate studied samples. (d) Parameter γ obtained from each adjustment.

efficiency is given by $Q_{ext}=(2/x^2)\Sigma(2n+1)\mathrm{Re}\{a_n+b_n\}$, where Re{} denotes the real part of the argument whereas a_n and b_n are extinction coefficients in the optical wavelengths, given in terms of Riccati-Bessel's functions $\psi_n(\rho)$ and $\xi_n(\rho)$ [73]:

$$a_n=\frac{M\psi_n(Mx)\psi_n'(x)-\psi_n(x)\psi_n'(Mx)}{M\psi_n(Mx)\xi_n'(x)-\xi_n(x)\psi_n'(Mx)},$$

$$b_n=\frac{\psi_n(Mx)\psi_n'(x)-M\psi_n(x)\psi_n'(Mx)}{\psi_n(Mx)\xi_n'(x)-M\xi_n(x)\psi_n'(Mx)}, \tag{8}$$

where prime ($'$) indicates differentiation with respect to the argument (ρ), $x=\pi D/\lambda$, and the relative refractive index M is given in terms of particle and medium electric permittivity: $M^2=\varepsilon_1/\varepsilon_m$. The Riccati-Bessel's functions can be obtained from $\psi_n=\rho j_n(\rho)$ and $\xi_n=\rho h_n^{(1)}(\rho)$, where j_n are spherical Bessel's functions of first type and $h_n^{(1)}$ are spherical Hankel's functions.

In order to take into account chain formation, we define an effective refractive index $M(Q)$ replacing χ_Q^{zz} in Clausius-Mossotti's relation:

$$M(Q)=\sqrt{\frac{2\chi_Q^{zz}+3}{3-\chi_Q^{zz}}}. \tag{9}$$

The zz component was chosen because chains tend to align along the applied magnetic field, at high-field values. From this point of view we were able to simulate the effect of chain formation in the Mie's resonance. Figure 6 shows the behavior of the calculated extinction efficiency for different chain lengths ($Q=1$, 2, 5, and 100 nanoparticles in the linear chain). Considering $\lambda=632$ nm and the magnetite param-

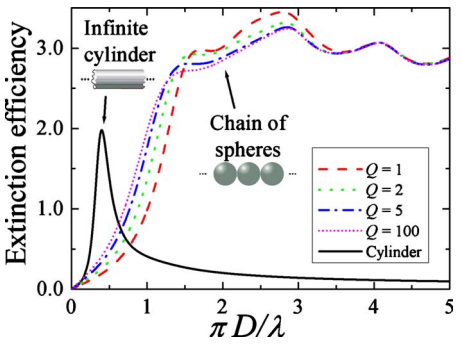

FIG. 6. (Color online) Extinction efficiency for Q chains formed by coated spheres and for an infinite cylinder which longitudinal axis makes 1° with incident electric field.

eters we found that the first Mie's resonance—the first maximum in extinction efficiency—occurs for monomers ($Q=1$) at a particle diameter of 344 nm whereas for pentamers ($Q=5$) we found the value of 312 nm in particle diameter. Even for a chain consisting of hundred of particles ($Q=100$), the Mie's resonance peaks do not shift significantly. Therefore, although the increase of the chain length leads to changes on the Mie's resonance positions, such phenomenon is not able to explain our data, since the modal size obtained for the MCs is two orders of magnitude smaller. Furthermore, using the Debye's theory [95] at optical wavelengths, one can show that the real and the imaginary parts of the magnetic susceptibility are both negligible. Therefore, although ferromagnetic scatterers represent an interesting idea, it seems that it plays no role in the present context. Since the fitting procedure using the power law does not provides exponents in the expected range, indicating that particles cannot work as magnetic scatterers in the studied wavelength, and also isolated chains are not able to produce Mie's resonance for particles smaller than 313 nm, a different physical phenomenon should be responsible for the minimum in the optical transmissivity.

A plausible origin for the critical field is a gas-liquid-like transition. Ivanov [42] used a thermodynamic model to investigate this phase transition in MF samples. The free energy for polydisperse magnetic particles suspended in a MF was modeled as [42]:

$$F = N_0\mu_0^o + \sum_i N_i\left(\mu_i^o + k_BT\ln\phi_i - k_BT\ln\frac{\sinh\xi_i}{\xi_i}\right) - k_BT\ F_{CS} - k_BT\sum_{i,j} N_i\phi_j G_{ij}, \tag{10}$$

where the index i indicates properties of the N_i nanoparticles with diameter D_i and volume fraction ϕ_i. μ_i^o is the chemical potential of an isolated magnetic particle and μ_0^o is the chemical potential of the pure carrier liquid consisting on N_0 molecules. As described in Ref. [96], F_{CS} is the free energy for a polydispersed hard-sphere gas, whose description is based on the Carnahan-Starling's equation of state. $\xi_i=\mu_0 m_i H/(k_BT)$ is the Langevin factor of each particle with magnetic moment $m_i=(\pi/6)D_i^3M_s$. Dipolar magnetic interaction among single particles' pairs is described via $G_{ij}=4\lambda_{ij}L(\xi_i)L(\xi_j)+(4/3)\lambda_{ij}^2$, with $\lambda_{ij}=8m_im_j/[k_BT(D_i+D_j+y)^3]$. The extra term y, not present in the original approach, was added because we considered a non-null distance between neighboring magnetic cores, due to the particle's surface coating layer. The particle size was modeled by a bidisperse system, presenting small and large particles. The diameter of small particles (D_1) was given by the average diameter of the distribution. The diameter of large particles (D_2) and their relative population were found in order to keep unchanged the averages $\langle D^3\rangle$ and $\langle D^6\rangle$ [42]. Using the Ivanov's model [42], we found for the TMF samples investigated $D_1=7.8$ nm (relative population of 96.4%) and $D_2=14.4$ nm. Likewise, for PMF samples we found $D_1=9.7$ nm (relative population of 95.5%) and $D_2=19.8$ nm. From Eq. (10) we obtained the chemical potential associated to both large and small particles. By detecting the presence of bends (analogous to the van der Waals loops) in the chemical potential as a function of particle volume fraction for given magnetic fields, we were able to build the phase diagram. Moreover, by using the surface-to-surface distance (y) between magnetic cores, as reported in Table I, we were able to simulate the evolution of the phase diagram induced by applied fields according to the Ivanov's model, as shown in Fig. 5(c). Our calculation shows that reduction of y leads to the decrease of H_c, in very good agreement with our experimental data. A qualitative comparison between phase diagram (lines) and experimental critical fields (symbols), both plotted in Fig. 5(c), shows that the dependence of H_c on ϕ is quite similar. However, phase transition is expected to occur in samples presenting particle volume fractions above the values actually used in our experiments. This difference may result from neglecting the existence of particle chains in the approach used and, consequently, the interaction between them. As long as bigger particles induce phase transition at lower ϕ values the presence of particle chains within TMF samples might be able to shift the phase diagram downwards. Nevertheless, the present theory does not take into account the existence and interaction of particle chains. Indeed, in a recent work Iskakova *et al.* [36] took into consideration the interaction among particle chains, though in their work comparison between MFs with and without particle chains was made only for monodisperse samples.

Regarding stable MC samples, as the applied magnetic field strength increases and becomes strong enough, particle chains might nucleate to form cylinderlike structures, a phenomenon known as columnar phase transition. The phenomenon has already been observed in two-dimensional MFs employing cryogenic transmission electron microscopy [20,37,38]; in ferrofluid emulsions [71], and in 2D systems possessing magnetic nanoparticles encapsulated in micron-sized polymer beads [97], both using optical microscopy; or even by naked eye as recently reported [19]. The critical magnetic field (H_c) above which this columnar phase transition occurs was estimated by equating the short-range direct interaction between particle chains and the fluctuation energy of a single particle chain within the column [71]:

$$H_c \approx A\left(\frac{\phi^\gamma}{G^2}\right)\exp\left(\frac{\pi G}{\phi^{\gamma/2}}\right), \tag{11}$$

where A is a constant that depends on both the dc magnetic permeability of the suspended particle and the liquid carrier

plus the particle diameter dispersity. The γ parameter reflects the sensitivity of the volume fraction dependence of the average distance between particle chains within the columns and G is a geometrical factor describing the particle chain arrangement within the column. Lines in Figs. 5(a) and 5(b) are the best fit of the experimental data (symbols) according to Eq. (11). We first fitted the 30-day-old sample data, from which we found $A=1.9\pm0.2$, $G=0.29\pm0.03$, and $\gamma=0.79\pm0.02$. Interestingly, the G parameter value we found was quite similar to the one reported for MF emulsions [71]. Then, to analyze the older samples we fixed the obtained A and G values. This procedure was chosen to better understand the physical process behind the phenomenon, since strong dependence was found among the three parameters. Figure 5(d) shows the γ parameter at different aging times, revealing reduction of the γ parameter as the aging time increases. Our results indicate that isolated particle chains approach each other within the columns as the sample aging increases, probably due to surface coating layer desorption [56,66], which is in agreement with our chain length analysis (see Table I). From the dependence of the average chain size upon the aging time and particle volume fraction, we conclude that longer particle chains help the nucleation process toward columns formation.

By modeling columns as infinite cylinders, one can find the cylinder's critical diameter at which Mie's resonance takes place. In this case the extinction efficiency of the cylinder (Q_{cyl}) is given by the ratio between the cylinder's extinction cross section and its orthogonal projected area ($L\times D_{cyl}$), where L and D_{cyl} are the cylinder's length and diameter, respectively. According to the literature, $Q_{cyl}=(2/x)\mathrm{Re}\{c_0+2\Sigma c_n\}$, where the coefficients c_n are given by [73]:

$$c_n = \frac{W_n B_n + iD_n C_n}{W_n V_n + iD_n^2},$$

$$B_n = \xi[M^2 \xi J_n'(\eta) J_n(\xi) - \eta J_n'(\eta) J_n'(\xi)],$$

$$C_n = n\cos\ \eta J_n(\eta) J_n(\xi)(\xi^2/\eta^2 - 1),$$

$$D_n = n\cos\ \eta J_n(\eta) H_n^{(1)}(\xi)(\xi^2/\eta^2 - 1),$$

$$V_n = \xi[M^2 \xi J_n'(\eta) H_n^{(1)}(\xi) - \eta J_n(\eta) H_n^{(1)'}(\xi)],$$

$$W_n = i\xi[\eta J_n(\eta) H_n^{(1)'}(\xi) - \xi J_n'(\eta) H_n^{(1)}(\xi)], \qquad (12)$$

with $\xi=x\sin\vartheta$, $\eta=x\sqrt{M^2-\cos^2\vartheta}$, $x=\pi D_{cyl}/\lambda$, J_n is first kind Bessel's functions, $H_n^{(1)}$ is first type Hankel's functions and ϑ denotes the angle between the cylinder's axis and the incident electric field. The coefficients described in Eq. (12) were used to calculate the extinction efficiency of an infinite cylinder (see Fig. 6), where the direction of the electric field of the incident light and the cylinder's axis are 1° off. Mie's resonance was found to occur around a critical diameter of 80 nm, indicating that for the MC samples investigated here about 10 particle chains can be placed side-by-side across the columns' diameter. This phenomenon could easily happen at the columnar phase transition.

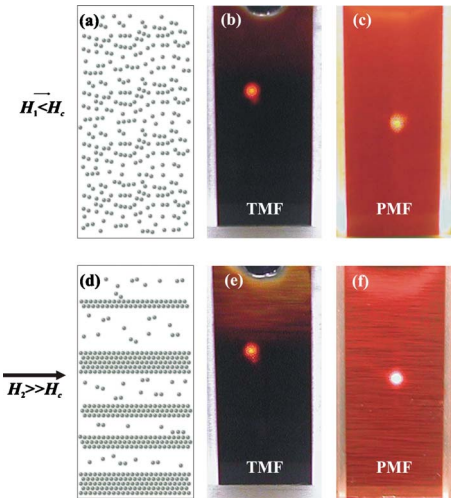

FIG. 7. (Color online) (a) Schematic of nanoparticle configuration in the carrier liquid and pictures of (b) TMF and (c) PMF samples for fields lower than the critical value ($H_1<H_c$) (d) Representation of nanoparticles configuration and pictures of (e) TMF and (f) PMF samples for very strong fields ($H_2\gg H_c$). For a low field, chains are oriented along magnetic field and the sample is homogeneous (a–c). At high fields, much stronger than H_c, smooth stripes could be seen in the samples, which are the columnar structures growing up and settling down (d–f).

Figure 7 reproduces the expected configurations of nanoparticles within a MC sample as the applied magnetic field (H) is compared to the critical field (H_c). For applied fields $H<H_c$ [see Fig. 7(a)], particle chains within the MC sample start to align along the applied field, leading to the decrease in relative transmission. Figures 7(b) and 7(c) shows pictures obtained from the TMF and PMF samples for low fields, supporting the scheme presented in Fig. 7(a). Then, for applied fields $H>H_c$, longer particle chains collapse into cylinderlike structures, incorporating smaller chains and monomers, forming long columns of particle chains and leading to a columnar phase transition. The columnar structures reach a critical diameter able to produce the Mie's resonances, being responsible for the minimum in the magneto-transmissivity experiment. Increasing even further the magnetic field ($H\gg H_c$) the columnar structures become thicker and heavier [see Fig. 7(d)]. As a consequence, the thick columnar structures start to flocculate, following precipitation under gravity. Figures 7(e) and 7(f) corresponds to the pictures of the TMF and PMF samples at magnetic fields much stronger that the critical value, where it can be observed, by naked eye, the presence of horizontal columnar structures, especially in the PMF sample [19].

We also studied the dependence of the relative transmission and, consequently, the critical field, as a function of the rate at which the applied magnetic field is increased. The 1460-day-old PMF samples, at different particle volume fractions, were investigated under four increasing magnetic field rate values (dH/dt). Figure 8(a) shows the relative transmission data for the most concentrated PMF sample ($\phi=1.52$). We found that the faster the magnetic field is increased from zero the higher the critical field observed. Interestingly, at the fastest field rate value employed

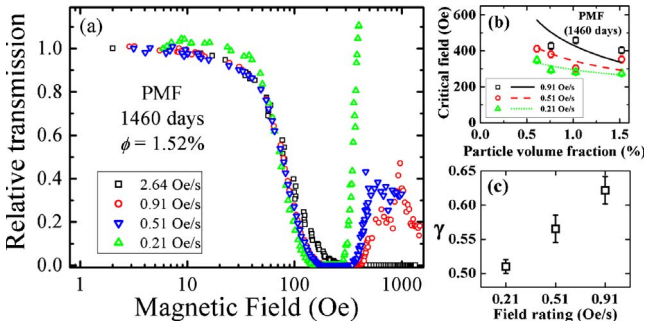

FIG. 8. (Color online) (a) Symbols show relative parallel transmissivity $t_{\|}$ for 1460-day-old PMF samples possessing ϕ=1.52 as function of magnetic field for different field ratings. (b) Symbols show H_c as function of particle volume fraction for 1460-day-old PMF samples at different field ratings. Lines are the fitting of experimental data according to the structural transition model (see Eq. (11)). (c) Parameter γ obtained from each adjustment.

(2.64 Oe/s) we observed no columnar phase transition [see Fig. 8(a)]. A similar behavior was found for other values of particle volume fractions investigated. Symbols in Fig. 8(b) show the particle volume fraction dependence of the critical field at different field rate values whereas the lines (solid, dashed, dotted) indicate the best fit of the experimental data according to Eq. (11). The geometrical factor describing the particle chain arrangement in a columnlike structure was fixed in G=0.29. Then, we fitted the data corresponding to the slowest field rate value employed (0.21 Oe/s), which is the one used on our previous measurements, resulting in $A=13.3\pm0.8$ and $\gamma=0.51\pm0.01$. In order to clarify the underlying physics and to fit the other two sets of data (0.51 and 0.91 Oe/s), we fixed the parameter A. The values of γ we found for different field rate values are shown in Fig. 8(c), revealing that the faster the increase of the applied field the higher the γ parameter. Our finding indicates that the rate at which the applied magnetic field increases influences the onset and the structure of field-induced particle chains and columns in MCs. This finding might be extremely important for biomedical applications of magnetic colloid-based materials, since preventing the onset of such structures might help avoid embolization in arteries and capillaries.

V. CONCLUSION

In conclusion, the magneto-transmissivity of aqueous colloid samples based on nanosized magnetite surface-coated with tartrate and polyaspartate were investigated. The theoretical model employed to analyze the data showed that rotation of pre-existing or field-induced chains of nanosized magnetite within the samples can be responsible for the observed decrease of transmitted light as the applied magnetic field increases. The analysis indicates that the average chain length increases as the sample's aging time increases, suggesting that magnetic colloids do not possess a static equilibrium configuration and surface-coating species have desorbed out from magnetite particles. At a critical field we found a minimum in the magneto-transmissivity, here identified as due to a columnar phase transition taking place within the magnetic colloid, in which isolated chains of particles bind together to form columnar-like structures. Although particle chain formation shifts the Mie's resonance peak position, the theory shows that the onset of columnar-like structures are more likely to explain the observed phase transition. Therefore, since such transition depends on the particle size and particle volume fraction concentration, the field-dependence of the magneto-transmissivity could be used to build magnetically tunable colloidal-based photonic devices. Moreover, we could establish the dependence of critical field on magnetic field rating, which has important implications on biomedical applications.

ACKNOWLEDGMENTS

We thank the Brazilian agencies CNPq, FINEP, and FUNAPE for financial support, Dr. Norbert Buske for providing the MC samples, Dr. Leandro Martin Socolovsky for the TEM measurements, and the National Synchroton Light Laboratory (LME-LNLS, Campinas, Brazil) for the use of the TEM facility.

[1] A. Ito, H. Honda, and T. Kobayashi, Cancer Immunol. Immunother **55**, 320 (2006).
[2] A. F. Bakuzis, K. Skeff Neto, P. P. Gravina, L. C. Figueiredo, P. C. Morais, L. P. Silva, R. B. Azevedo, and O. Silva, Appl. Phys. Lett. **84**, 2355 (2004).
[3] H. E. Horng, C. S. Chen, K. L. Fang, S. Y. Yang, J. J. Chieh, C.-Y. Hong, and H. C. Yang, Appl. Phys. Lett. **85**, 5592 (2004).
[4] S. Pu, X. Chen, Z. Di, and Y. Xia, J. Appl. Phys. **101**, 053532 (2007).
[5] J. J. Chieh, S. Y. Yang, H. E. Horng, C.-Y. Hong, and H. C. Yang, Appl. Phys. Lett. **90**, 133505 (2007).
[6] W. Liao, X. Chen, Y. Chen, S. Pu, Y. Xia, and Q. Li, Appl. Phys. Lett. **87**, 151122 (2005).
[7] S. J. DeNardo, G. L. DeNardo, A. Natarajan, L. A. Miers, A. R. Foreman, C. Gruettner, G. N. Adamson, and R. Ivkov, J. Nucl. Med. **48**, 437 (2007).
[8] C. L. Dennis, A. J. Jackson, J. A. Borchers, P. J. Hoopes, R. Strawbridge, A. R. Foreman, J. van Lierop, C. Gruttner, and R. Ivkov, Nanotechnology **20**, 395103 (2009).
[9] T. Du, S. Yuan, and W. Luo, Appl. Phys. Lett. **65**, 1844 (1994).
[10] J. Liu, E. M. Lawrence, A. Wu, M. L. Ivey, G. A. Flores, K. Javier, J. Bibette, and J. Richard, Phys. Rev. Lett. **74**, 2828 (1995).
[11] W. Luo, T. Du, and J. Huang, Phys. Rev. Lett. **82**, 4134 (1999).
[12] F. A. Pinheiro, A. S. Martinez, and L. C. Sampaio, Phys. Rev. Lett. **84**, 1435 (2000); **85**, 5563 (2000).
[13] R. V. Mehta, R. Patel, R. Desai, R. V. Upadhyay, and K.

Parekh, Phys. Rev. Lett. **96**, 127402 (2006).
[14] R. V. Mehta, R. Patel, and R. V. Upadhyay, Phys. Rev. B **74**, 195127 (2006).
[15] J. Philip, J. M. Laskar, and B. Raj, Appl. Phys. Lett. **92**, 221911 (2008).
[16] J. M. Laskar, J. Philip, and B. Raj, Phys. Rev. E **78**, 031404 (2008).
[17] C. Z. Fan, G. Wang, and J. P. Huang, J. Appl. Phys. **103**, 094107 (2008).
[18] S. Pu, T. Geng, X. Chen, X. Zeng, M. Liu, and Z. Di, J. Magn. Magn. Mater. **320**, 2345 (2008).
[19] E. R. Cintra, J. L. Santos, Jr., L. M. Socolovsky, N. Buske, and A. F. Bakuzis, J. Magn. Magn. Mater. **320**, e351 (2008).
[20] P. Goldberg, J. Hansford, and P. J. Heerden, J. Appl. Phys. **42**, 3874 (1971).
[21] C. F. Hayes, J. Colloid Interface Sci. **52**, 239 (1975).
[22] E. A. Peterson and D. A. Krueger, J. Colloid Interface Sci. **62**, 24 (1977).
[23] J.-C. Bacri, R. Perzynski, D. Salin, V. Cabuil, and R. Massart, J. Colloid Interface Sci. **132**, 43 (1989).
[24] R. Massart, E. Dubois, V. Cabuil, and E. Hasmonay, J. Magn. Magn. Mater. **149**, 1 (1995).
[25] W. E. L. Haas and J. E. Adams, Appl. Phys. Lett. **27**, 571 (1975).
[26] W. Reed and J. H. Fendler, J. Appl. Phys. **59**, 2914 (1986).
[27] A. O. Tsebers, Magnetohydrodynamics **18**, 137 (1982).
[28] K. Sano and M. Doi, J. Phys. Soc. Jpn. **52**, 2810 (1983).
[29] Y. A. Buyevich and A. O. Ivanov, Physica A **190**, 276 (1992).
[30] A. O. Tsebers, Magnetohydrodynamics **28**, 24 (1992).
[31] A. Y. Zubarev and A. O. Ivanov, Phys. Rev. E **55**, 7192 (1997).
[32] A. Y. Zubarev and A. O. Ivanov, Physica A **251**, 332 (1998).
[33] D. Lacoste and T. C. Lubensky, Phys. Rev. E **64**, 041506 (2001).
[34] J. Richardi, D. Ingert, and M. P. Pileni, Phys. Rev. E **66**, 046306 (2002).
[35] A. Y. Zubarev and L. Y. Iskakova, Phys. Rev. E **65**, 061406 (2002).
[36] L. Y. Iskakova, G. A. Smelchakova, and A. Y. Zubarev, Phys. Rev. E **79**, 011401 (2009).
[37] M. Klokkenburg, B. H. Erne, J. D. Meeldijk, A. Wiedenmann, A. V. Petukhov, R. P. A. Dullens, and A. P. Philipse, Phys. Rev. Lett. **97**, 185702 (2006).
[38] M. Klokkenburg, B. H. Erne, A. Wiedenmann, A. V. Petukhov, and A. P. Philipse, Phys. Rev. E **75**, 051408 (2007).
[39] J. Richardi, M. P. Pileni, and J.-J. Weis, Phys. Rev. E **77**, 061510 (2008).
[40] J. Jordanovic and S. H. L. Klapp, Phys. Rev. E **79**, 021405 (2009).
[41] J. J. Weis, Mol. Phys. **103**, 7 (2005).
[42] A. O. Ivanov, J. Magn. Magn. Mater. **154**, 66 (1996).
[43] J. Liu, G. A. Flores, and R. Sheng, J. Magn. Magn. Mater. **225**, 209 (2001).
[44] G. A. Flores, R. Sheng, and J. Liu, J. Intell. Mater. Syst. Struct. **10**, 708 (1999).
[45] G. A. Flores and J. Liu, J. Intell. Mater. Syst. Struct. **13**, 641 (2002).
[46] P. C. Scholten, IEEE Trans. Magn. **16**, 221 (1980).
[47] A. Y. Zubarev and L. Y. Iskakova, Phys. Rev. E **61**, 5415 (2000).
[48] A. Y. Zubarev and L. Y. Iskakova, Phys. Rev. E **76**, 061405 (2007).
[49] V. S. Mendelev and A. O. Ivanov, Phys. Rev. E **70**, 051502 (2004).
[50] A. O. Ivanov, Z. Wang, and C. Holm, Phys. Rev. E **69**, 031206 (2004).
[51] A. Y. Zubarev and L. Y. Iskakova, Phys. Rev. E **68**, 061203 (2003).
[52] P. G. DeGennes and P. A. Pincus, Phys. Kondens. Mater. **11**, 189 (1970).
[53] P. C. Jordan, Mol. Phys. **25**, 961 (1973).
[54] A. O. Tsebers, Magnetohydrodynamics **10**, 135 (1974).
[55] L. L. Castro, M. F. da Silva, A. F. Bakuzis, and R. Miotto, J. Magn. Magn. Mater. **293**, 553 (2005).
[56] L. L. Castro, G. R. R. Gonçalves, K. S. Neto, P. C. Morais, A. F. Bakuzis, and R. Miotto, Phys. Rev. E **78**, 061507 (2008).
[57] E. R. Cintra, F. S. Ferreira, J. L. Santos, Jr., J. C. Campello, L. M. Socolovsky, E. M. Lima, and A. F. Bakuzis, Nanotechnology **20**, 045103 (2009).
[58] R. W. Chantrell, A. Bradbury, J. Popplewell, and S. W. Charles, J. Appl. Phys. **53**, 2742 (1982).
[59] P. J. Camp, J. C. Shelley, and G. N. Patey, Phys. Rev. Lett. **84**, 115 (2000).
[60] A. Ghazali and J. C. Levy, Phys. Rev. B **67**, 064409 (2003).
[61] T. Kruse, H.-G. Krauthäuser, A. Spanoudaki, and R. Pelster, Phys. Rev. B **67**, 094206 (2003).
[62] T. Kristóf and I. Szalai, Phys. Rev. E **68**, 041109 (2003).
[63] K. Skeff Neto, A. F. Bakuzis, G. R. R. Goncalves, F. Pelegrini, and P. C. Morais, J. Magn. Magn. Mater. **289**, 129 (2005).
[64] A. F. Bakuzis, A. F. da Silva, P. C. Morais, L. S. F. Olavo, and K. Skeff Neto, J. Appl. Phys. **87**, 2497 (2000).
[65] S. Taketomi, M. Ukita, M. Mizukami, H. Miyajima, and S. Chikazumi, J. Phys. Soc. Jpn. **56**, 3362 (1987).
[66] M. T. A. Eloi, R. B. Azevedo, E. C. D. Lima, A. C. M. Pimenta, and P. C. Morais, J. Magn. Magn. Mater. **293**, 220 (2005).
[67] S. P. Leary, C. Y. Liu, and M. L. J. Apuzzo, Neurosurgery **58**, 1009 (2006).
[68] J. W. M. Bulte, T. Douglas, B. Witwer, S. C. Zhang, E. Strable, B. K. Lewis, H. Zywicke, B. Miller, P. van Gelderen, B. M. Moskowitz, I. D. Duncan, and J. A. Frank, Nat. Biotechnol. **19**, 1141 (2001).
[69] H. Wang, Y. Zhu, C. Boyd, W. Luo, A. Cebers, and R. E. Rosensweig, Phys. Rev. Lett. **72**, 1929 (1994).
[70] C.-Y. Hong, H. E. Horng, F. C. Kuo, S. Y. Yang, H. C. Yang, and J. M. Wu, Appl. Phys. Lett. **75**, 2196 (1999).
[71] M. Ivey, J. Liu, Y. Zhu, and S. Cutillas, Phys. Rev. E **63**, 011403 (2000).
[72] G. Mie, Ann. Phys. **25**, 377 (1908).
[73] C. F. Bohren and D. R. Huffman, *Absorption and Scattering of Light by Small Particles* (Wiley, New York, 1983).
[74] J. B. Jackson and N. J. Halas, J. Phys. Chem. B **105**, 2743 (2001).
[75] P. K. Jain, I. H. El-Sayed, and M. A. El-Sayed, Nanotoday **2**, 18 (2007).
[76] A. O. Govorov and H. H. Richardson, Nanotoday **2**, 30 (2007).
[77] C. Rockstuhl, F. Lederer, C. Etrich, T. Pertsch, and T. Scharf, Phys. Rev. Lett. **99**, 017401 (2007).
[78] J. H. Lee, Q. Wu, and W. Park, Opt. Lett. **34**, 443 (2009).

[79] L. Wang, J. Luo, Q. Fan, M. Suzuki, I. S. Suzuki, M. H. Engelhard, Y. Lin, N. Kim, J. Q. Wang, and C.-J. Zhong, J. Phys. Chem. B **109**, 21593 (2005).
[80] Z. Xu, Y. Hou, and S. Sun, J. Am. Chem. Soc. **129**, 8698 (2007).
[81] P. Gong, H. Li, X. He, K. Wang, J. Hu, W. Tan, S. Zhang, and X. Yang, Nanotechnology **18**, 285604 (2007).
[82] H. Chen, A. D. Ebner, A. J. Rosengart, M. D. Kaminski, and J. A. Ritter, J. Magn. Magn. Mater. **284**, 181 (2004).
[83] A. J. Rosengart, M. D. Kaminski, H. Chen, P. L. Caviness, A. D. Ebner, and J. A. Ritter, J. Magn. Magn. Mater. **293**, 633 (2005).
[84] J. D. Goff, P. P. Huffstetler, W. C. Miles, N. Pothayee, C. M. Reinholz, S. Ball, R. M. Davis, and J. S. Riffle, Chem. Mater. **21**, 4784 (2009).
[85] M. A. G. Soler, E. C. D. Lima, S. W. da Silva, T. F. O. Melo, A. C. M. Pimenta, J. P. Sinnecker, R. B. Azevedo, V. K. Garg, A. C. Oliveira, M. A. Novak, and P. C. Morais, Langmuir **23**, 9611 (2007).
[86] M. Strömberg, K. Gunnarsson, S. Vaqlizadeh, P. Svedlindh, and M. Strømme, J. Appl. Phys. **101**, 023911 (2007).
[87] D. Gunter and N. Buske, DE Patent No. 4325386 (16 August 1993).
[88] K. Aurich, M. Schwalbe, J. H. Clement, W. Weitschies, and N. Buske, J. Magn. Magn. Mater. **311**, 1 (2007).
[89] W. F. J. Fontijn, P. J. van der Zaag, M. A. C. Devillers, V. A. M. Brabers, and R. Metselaar, Phys. Rev. B **56**, 5432 (1997).
[90] D. R. Lide, *Handbook of Chemistry and Physics*, 87th ed. (C.R.C. Press, Boca Raton, 2007).
[91] K. Butter, P. H. H. Bomans, P. M. Frederik, G. J. Vroege, and A. P. Philipse, Nature Mater. **2**, 88 (2003).
[92] M. Xu and P. J. Ridler, J. Appl. Phys. **82**, 326 (1997).
[93] G. D. Benicio, F. Pelegrini, A. F. Bakuzis, K. L. C. Miranda, and P. P. C. Sartoratto, J. Appl. Phys. **101**, 09J106 (2007).
[94] R. E. Rosensweig, *Ferrohydrodynamics* (Dover, New York, 1997).
[95] R. E. Rosensweig, J. Magn. Magn. Mater. **252**, 370 (2002).
[96] G. A. Mansoori, N. F. Carnahan, K. E. Starling, and T. W. Leland, Jr., J. Chem. Phys. **54**, 1523 (1971).
[97] L. E. Helseth, J. Phys. D **42**, 105005 (2009).